PICASSO VISION instrument design, Engineering Model test results and Flight Model development status

Antti Näsilä*[a], Christer Holmlund[a], Rami Mannila[a], Ismo Näkki[a], Harri J. Ojanen[a], Altti Akujärvi[a], Heikki Saari[a], Didier Fussen[b], Didier Pieroux[b], Philippe Demoulin[b]
[a]VTT Technical Research Centre of Finland Ltd., Tietotie 3, FI 02044 Espoo, (Finland)
[b]Belgian Institute for Space Aeronomy, Avenue Circulaire 3, 1180 Uccle, (Belgium)

ABSTRACT

PICASSO - A PICo-satellite for Atmospheric and Space Science Observations is an ESA project led by the Belgian Institute for Space Aeronomy, in collaboration with VTT Technical Research Centre of Finland Ltd, Clyde Space Ltd. (UK) and Centre Spatial de Liège (BE). The test campaign for the engineering model of the PICASSO VISION instrument, a miniaturized nanosatellite spectral imager, has been successfully completed. The test results look very promising. The proto-flight model of VISION has also been successfully integrated and it is waiting for the final integration to the satellite platform.

Keywords: CubeSat, spectral imaging, Fabry-Perot, atmospheric remote sensing

1. INTRODUCTION

PICASSO - A PICo-satellite for Atmospheric and Space Science Observations is an ESA project led by the Belgian Institute for Space Aeronomy, in collaboration with VTT Technical Research Centre of Finland Ltd, Clyde Space Ltd. (UK), and the Centre Spatial de Liège (BE). PICASSO is a three-unit CubeSat, for which VTT develops the main payload: the Visible Spectral Imager for Occultation and Nightglow (VISION). VISION primarily targets the observation of the Earth's atmospheric limb during orbital Sun occultation. By assessing the radiation absorption in the Chappuis band for different tangent altitudes, the vertical profile of the ozone can be retrieved. A secondary objective is to measure the deformation of the solar disk so that stratospheric and mesospheric temperature profiles are retrieved by inversion of the refractive ray-tracing problem. The measurement scenario is illustrated in Figure 1.[1]

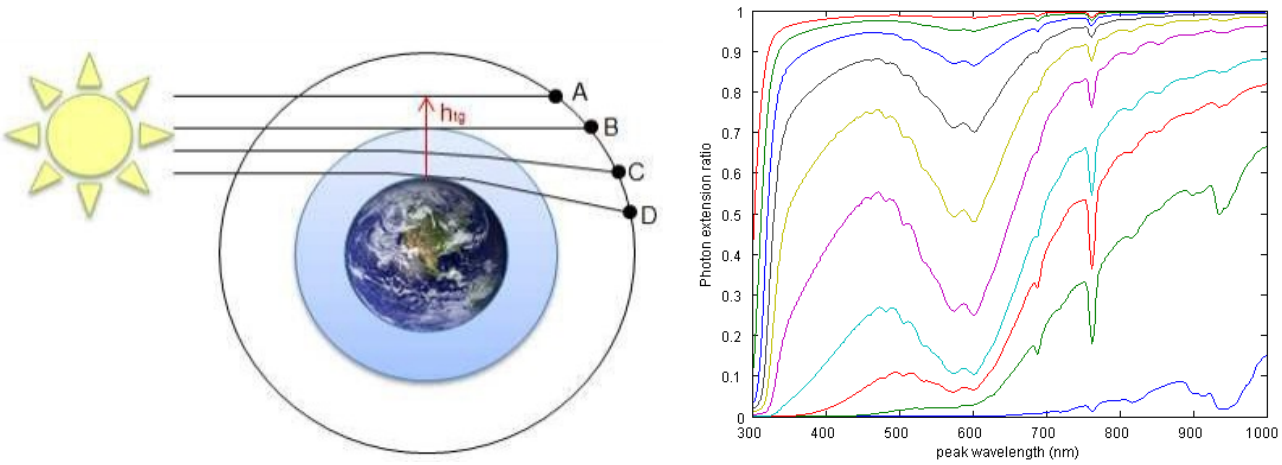

Figure 1. Left: The measurement scenario for sunset occultation. The reference observation is taken at position A and the measurements are performed at positions B-D as the sun moves behind the horizon. Right: The spectral photon depletion at altitudes between 50 km down to 5 km.

*antti.nasila@vtt.fi; phone +358 40 671 6266; www.vttresearch.com

Remote Sensing of Clouds and the Atmosphere XXI, edited by Adolfo Comerón, Evgueni I. Kassianov, Klaus Schäfer, James W. Jack, Richard H. Picard, Konradin Weber, Proc. of SPIE Vol. 10001, 1000109 · © 2016 SPIE · CCC code: 0277-786X/16/$18 · doi: 10.1117/12.2241956

The VISION instrument is a small (ca. 10 cm x 10 cm x 5 cm) and lightweight (ca. 500 g) spectral imager operating in the visible and near-infrared domain (430 – 800 nm). It is capable of taking 2D snapshots at freely selectable wavelengths within this range. VISION total field of view is 2.5°x 2.5° and it delivers 1024 x 1024 pixel (2048 x 2048 RGB pixels) spectral images; as the angular size of the sun is ca. 0.5°, the size of the solar disk is about 200 pixel-wide. The spectral separation is done by a tunable Fabry-Perot interferometer which has spectral resolution better than 10 nm (FWHM).[2]

The Fabry-Pérot interferometer (FPI) consists of two reflective surfaces separated by an air gap (Figure 2), which act as an optical resonator. By tuning the air gap, the center wavelength of the passbands can be adjusted. In VISION, the air gap tuning is done by three piezo actuators. The passband wavelength is defined by[3]

$$m\lambda = 2nd\cos\theta, \tag{1}$$

where m is the order of the passband (1, 2, 3…), λ is the wavelength, n is the refraction index of the medium between the mirrors, d is the air gap width and θ is the ray angle in the air gap. The transmission bandwidth depends on the order of the passband and the reflectance of the mirrors: a narrow spectral bandwidth can be achieved with highly reflective mirrors and by using high orders of the FPI. Example of the FPI transmission spectrum is shown on the right side of Figure 2.

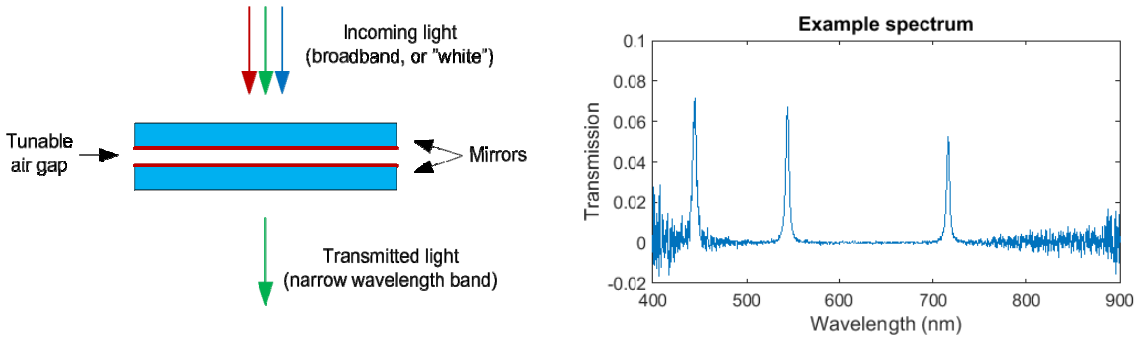

Figure 2. Left: Illustration of the Fabry-Pérot Interferometer. Right: An example of a measured transmission spectrum. The increased noise at both ends of the spectrum is caused by the decreased sensitivity of the reference spectrometer (Ocean Optics HR4000).

Table 1. Main instrument parameters

Parameter	Value	notes
Field of view	2.5° x 2.5°	
Image size	2048 x 2048 RGB pixels	1024 x 1024 spectral pixels
Spectral range	430 nm – 800 nm	
Spectral resolution @ FWHM	< 10 nm over the whole spectral range	
Mass	526 g	
Power consumption	< 3W	

2. INSTRUMENT DESIGN

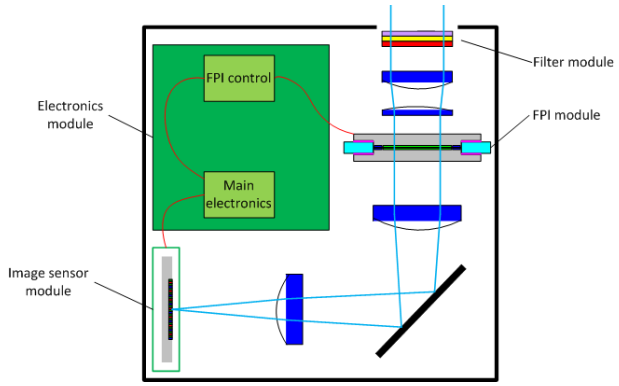

Figure 3. Basic functional diagram of the VISION instrument. The dimensions are 9.7 cm x 9.7 cm.

The VISION instrument consists of the following operational blocks (Figure 3):

- **The main electronics module,** which handles the image sensor readout and communication to the payload computer.
- **The FPI control electronics,** which handles the control loop for the FPI air gap. This module also creates the required voltages for the FPI piezo actuators.
- **FPI module,** which has the FPI element and the proximity electronics for the capacitive air gap measurement.
- **Image sensor module,** which consists of a commercial-off-the-shelf RGB CMOS image sensor (CMV4000 by CMOSIS)
- **Optics module,** which consists of 4 lens elements, a folding mirror, the short and longpass filters and a neutral density filter. The focal length of the optics is 248 mm and the F-number is 27. The optics is designed in a way that the light is collimated through the FPI to reduce spectral broadening caused by different ray angles.

The key component of VISION is the Fabry-Perot interferometer and the control electronics. As the FPI air gap width defines the transmitted wavelength, it is absolutely necessary to be able to control the width with good precision and stability. This is achieved by measuring the capacitance between electrodes deposited on the FPI mirror substrates. The capacitances are measured between three sets of electrodes positioned around the FPI mirrors and actuation is performed by three piezo-electric actuators mounted between the mirrors near the measurement electrodes. The capacitances are measured using a half-bridge configuration (Figure 4). The half-bridge consists of a reference capacitor (C_{ref}) and the changing capacitance between the FPI mirrors (C_m). The bridge is fed by two voltages, V_{ref}, and V_{sp}. V_{ref} is constant and common for all three control channels and the V_{sp} is set to match the wanted air gap. The voltage V_{sp} is usually called set point voltage or just set point. Voltage V_e represents the imbalance or error voltage which differs from zero if the balance condition ($V_{ref}C_{ref} = V_{sp}C_m$) is not met. When the error voltage differs from zero, the actuators will tune the air gap until the balance condition is achieved, thus resulting in a stable air gap.

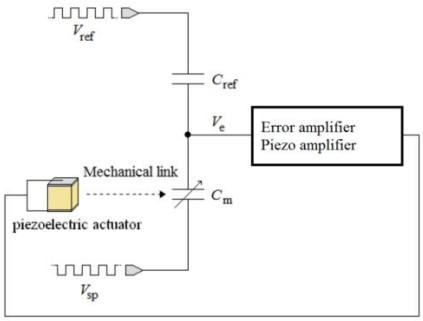

Figure 4. One of the three control loops for the FPI air gap control

In order to use the FPI as a spectral bandpass filter, the optical design chain has to be designed exactly for this purpose. As stated in equation 1, the angle of the rays entering the FPI affects the transmitted wavelength. In practice, this means that transmission peak broadens, as light goes through the FPI at different angles at different locations of the aperture. To

mitigate the broadening, the ray angles must be controlled. The straightforward way to do this is to collimate the light before it enters the FPI. This type of design is also used in VISION.

The image sensor used in VISION is a standard 4 megapixel RGB CMOS sensor, CMV4000 by CMOSIS. An RGB sensor is required because due to the FPI characteristics, at least two spectral bands are simultaneously transmitted within the spectral range. As RGB sensors have pixels with three different spectral responses, it is possible to calibrate the instrument for measuring up to three bands simultaneously[4]. The image sensor data is read out by an FPGA and transmitted directly to the payload computer over a high-speed LVDS interface.

Simply put, VISION will take images of the solar disk at a single wavelength and transfer the data directly to the payload computer. The wanted wavelength is selected by adjusting the FPI air gap to the desired transmission wavelength prior to imaging operations. The complete imaging sequence including data transfer takes less than 0.1 seconds for a single wavelength.

3. ENGINEERING MODEL TEST RESULTS

Introduction

An extensive test campaign was performed for the VISION Engineering Model (EM). The tests included FPI control accuracy and repeatability tests in vacuum, thermal stability tests in both air and vacuum, pointing stability test in thermal vacuum, spectral resolution and spectral stability tests in thermal vacuum. In addition to the thermal vacuum tests, vibration and shock testing was performed to VISION-EM according to the General Environmental Verification Standard GSFC-STD-7000.

Most of the optical characterization tests were performed using the dedicated optical ground support equipment (OGSE), which is shown in Figure 5. VISION OGSE uses an achromatic lens to collimate the light from the target to mimic infinite imaging distance, as VISION is focused to infinity. The target can be either a slit target for line spread function measurement or a sun-like target for resolution and spectral response characterization.

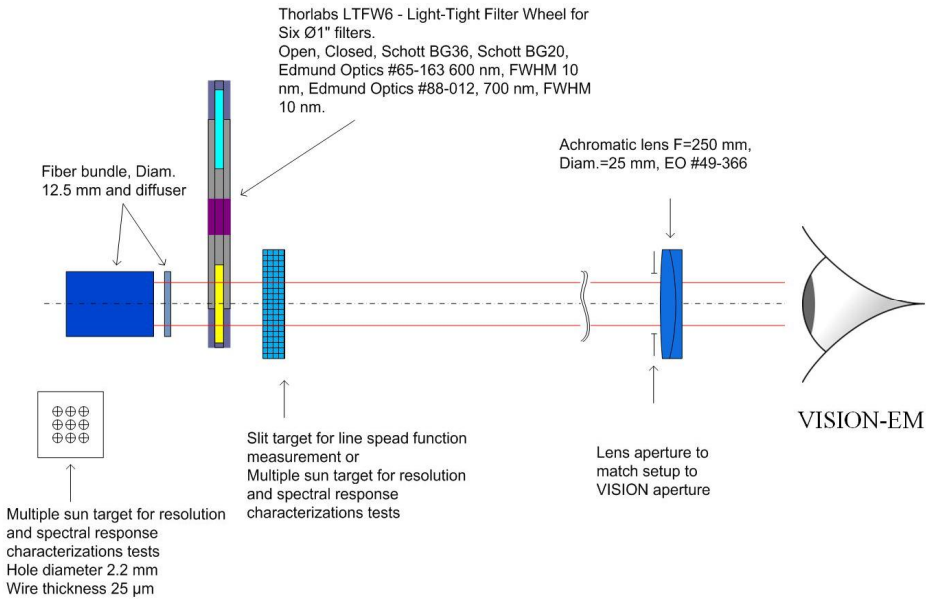

Figure 5. VISION OGSE optical concept.

FPI step response

As the imaging rate is very high in the Picasso mission, it was necessary to characterize the settling time of the FPI. This was required measuring the closed loop step response in vacuum. This was done by measuring the transmission spectrum of the FPI and then correlating the spectrum against simulations to find out the physical air gap corresponding to the measured spectrum[5]. The measurement was repeated at 0.1 ms intervals during a 10 nm step. The result is shown in Figure 6, and it can be seen that the FPI stabilization time is ca. 20 ms. The measurement was performed in room temperature and the air gap was measured from the center of the optical aperture.

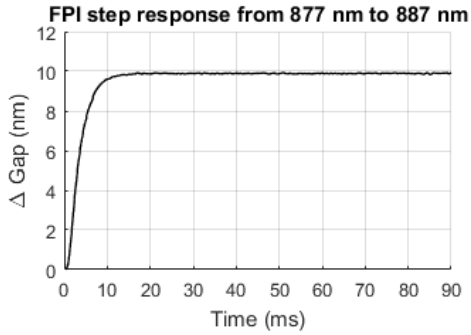

Figure 6. The closed loop step response for the FPI. The air gap step was from 877 nm to 887 nm.

FPI air gap repeatability

In addition to the FPI control accuracy, the FPI air gap repeatability must also be adequate. This was measured by adjusting the set point voltage to different values in random order and measuring the transmitted wavelengths. The measurement data is shown in Figure 7, where the transmitted wavelengths as a function of set point voltage and the standard deviation for each set point are shown. Although there are some erroneous measurements, the standard deviation for each set point is less than 0.5 nm (mean value 0.18 nm), thus the repeatability is satisfactory. This measurement was performed in thermal chamber in a dry nitrogen atmosphere and at +30 °C. After excluding the erroneous measurements, 9538 data points were used for the repeatability assessment.

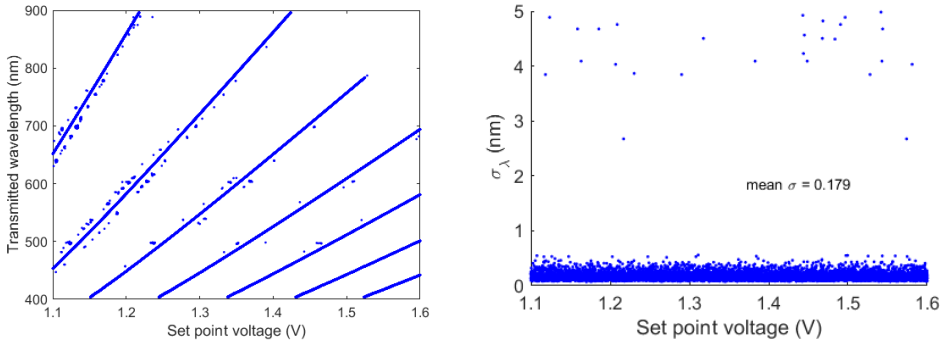

Figure 7. Left: The transmitted wavelengths for different interference orders as a function of set point voltage. Right: The standard deviation of the transmitted wavelength for each set point. Mostly the standard deviation is below 1 nm, but as the set point voltages were chosen at random, some voltages do not have enough measurement points for proper analysis, thus the standard deviation is higher at some points.

Spectral performance and stability

The performance of the previous instrument, the Aalto-1 Spectral Imager, was sensitive to low temperatures[5], thus the FPI design was revised for Picasso VISION. During the thermal vacuum test campaign, the instrument function behavior was measured between -35°C and +65°C to ensure that the performance is not degrading. The instrument function was measured by illuminating the VISION-EM with a low-pressure Hg-lamp combined with a 5 nm bandpass filter at 546 nm.

With this setup, only a single, extremely narrow, spectral line was used for the illumination. The narrow Hg-line spectrum was then measured with VISION-EM, thus effectively giving the instrument function, as shown in Figure 8.

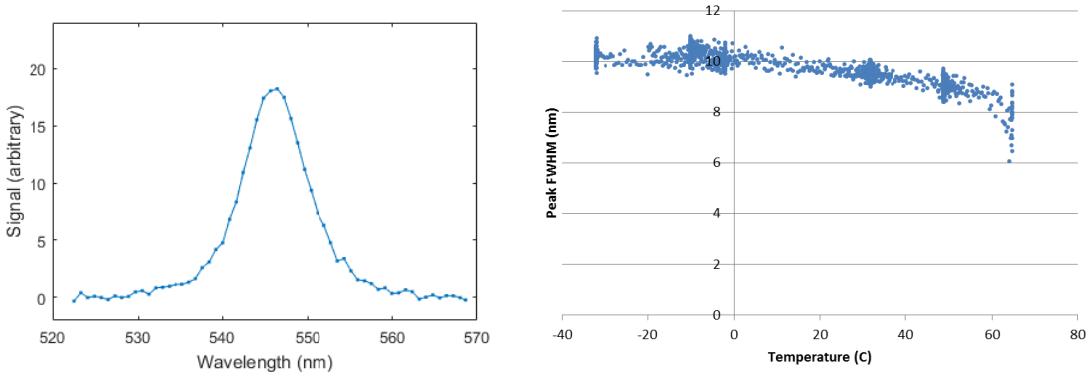

Figure 8. Left: An example of a Hg-lamp spectrum measured with VISION-EM. The FHWM is ca. 10 nm. Right: The FWHM of the first order instrument function at different temperatures.

The measurements were performed continuously as the temperature was cycled between -35°C and +65°C. Figure 8 shows the FWHM of the instrument function as a function of temperature. Some variation is present, but generally the FWHM remains at or below 10 nm. The same measurement setup was also used to measure the wavelength drift with respect to temperature as the wavelength of the Hg lamp spectral line is well known and quite stable. As the instrument function was measured, the transmission peak was recorded at different set point voltages at different temperatures. The set point voltage required to achieve the same wavelength as the Hg lamp at different temperatures is shown in Figure 9.

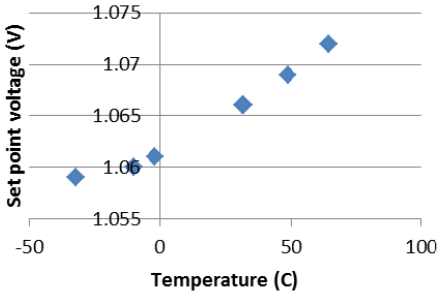

Figure 9. The set point voltage required for achieving the same air gap (or wavelength). The set point voltage corresponds to the same physical air gap, as the narrow Hg-line is exactly at 546 nm.

The effect of this drift is seen in Figure 10, where a known spectral target, a BG20 filter, has been measured at different temperatures. The figure also includes a reference measurement of the filter transmission.

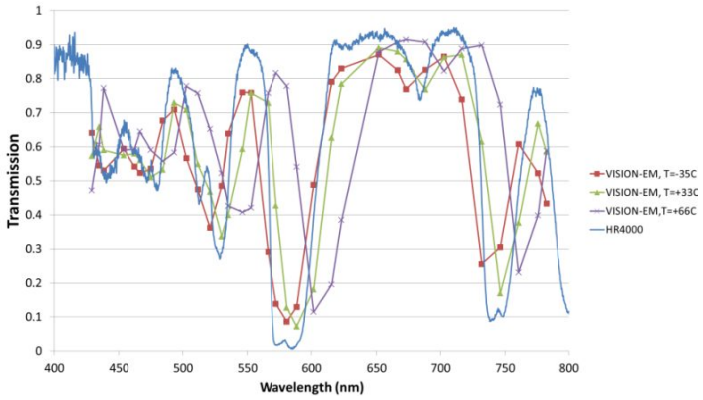

Figure 10. Measurement of a BG20 filter, measured at three different temperatures. Reference measurement done with Ocean Optics HR4000 spectrometer.

On-board calibration method verification

The VISION instrument also has a possibility to perform wavelength calibration in-flight. This is done by measuring the position of the short- or longpass filter edge. This is done by measuring the sun (or any other target) and scanning the FPI transmission peak over the filter edge. The location of the filter edge is visible as a clear drop or rise in the signal level. This can be done, as the filter edge location is much less sensitive to temperature than the FPI. By combining this measurement with the atmospheric measurements, each observation can be adjusted to the correct wavelength. This calibration can be called EDGE calibration.

The setup for the measurement is shown in Figure 11, where a known spectral target (BG20 filter) was placed outside the temperature chamber. In the test, two measurements were performed at different temperatures: first the halogen lamp spectrum was measured without the BG20 filter and the FPI transmission peak was scanned over the short and long pass filters of VISION. After this, the BG20 filter was added in front of the lamp and its transmission spectrum was measured. The measurements were repeated every 10 degrees between -40 °C and +50 °C.

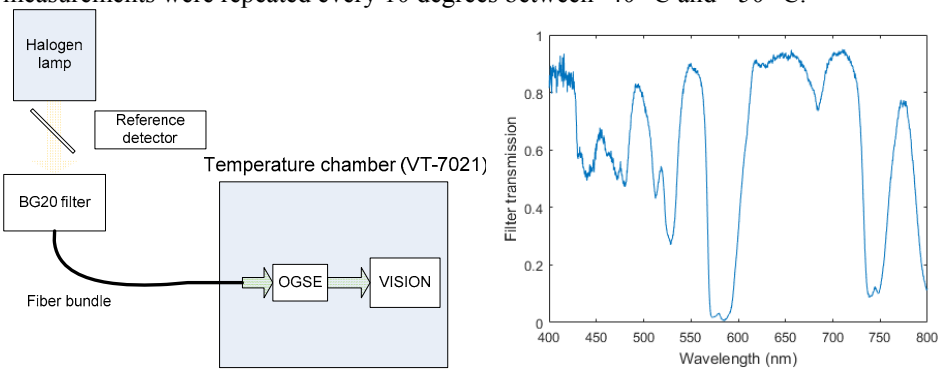

Figure 11. Left: The measurement setup for the test. VISION and the OGSE were placed inside a temperature chamber, while the lamp and the spectral target were outside the chamber. Right: The BG20 filter transmission measured with a reference spectrometer (Ocean Optics HR4000)

The measurement results are shown in Figure 12 and Figure 13. Without the EDGE calibration, the filter spectrum drifts with temperature roughly 30 nm over the whole temperature range, but with the calibration, the peak-to-peak drift drops to 3 nm. Overall the standard deviation of the absorption band locations drops to less than 1 nm.

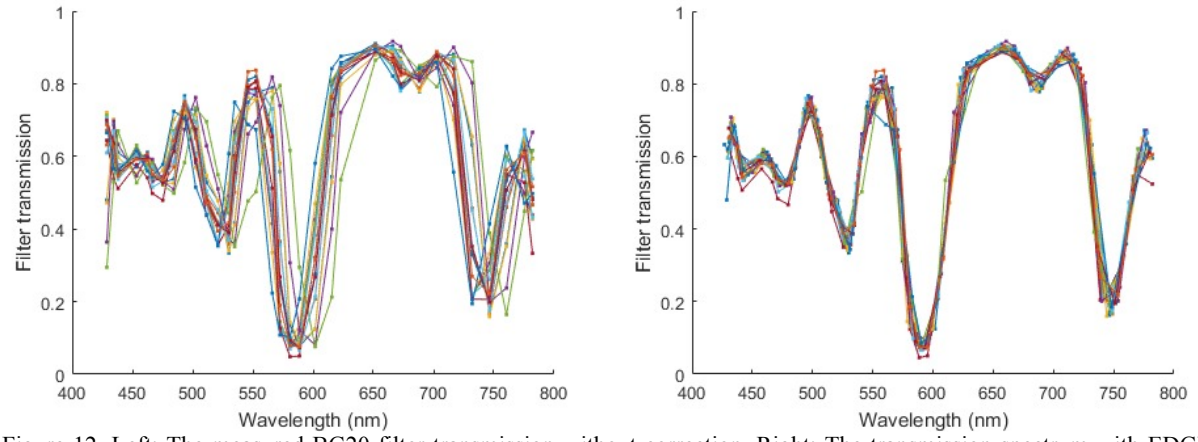

Figure 12. Left: The measured BG20 filter transmission without correction. Right: The transmission spectrum with EDGE correction applied.

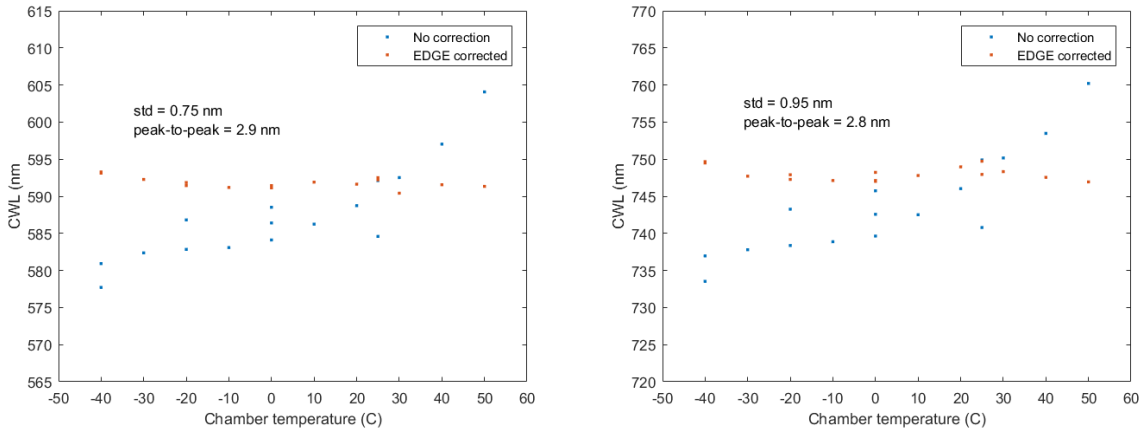

Figure 13. The location of BG20 filter absorption bands with (red) and without the EDGE correction (blue). With the correction enabled, wavelength shift caused by temperature can be compensated almost completely. With the edge correction the maximum deviation of the absorption bands is less than 3 nm with a standard deviation less than 1 nm.

Optical MTF

The MTF test procedure was based on the measurement of the line spread function of the VISION-EM with 5 µm wide 3.00 ± 0.025 mm long slit target at the optical axis of the VISION OGSE. From this test result it was possible to calculate the MTF on the optical axis. The MTF at the other locations of the image is retrieved from the measured line spread functions of the 25 µm thick platinum wire targets of the VISION OGSE.

VISION-EM image of the 5 µm wide, 3.00 ± 0.025 mm long slit target at the optical axis in vacuum at the temperature of 30 C is shown in Figure 14. For green pixels the FPI is set to the air gap value 367 ± 1 nm transmitting the wavelength 546.0 ± 1 nm and with spectral resolution of 11.5 nm @ FWHM. For Red and Blue pixels FPI air gap was set the value 537 ± 1 nm transmitting wavelengths 484.4 ± 1 nm and 702.7 ± 1 nm. The VISION instrument MTF requirement is also plotted in Figure 15. VISION-EM MTF performance was found to be compliant with instrument requirements.

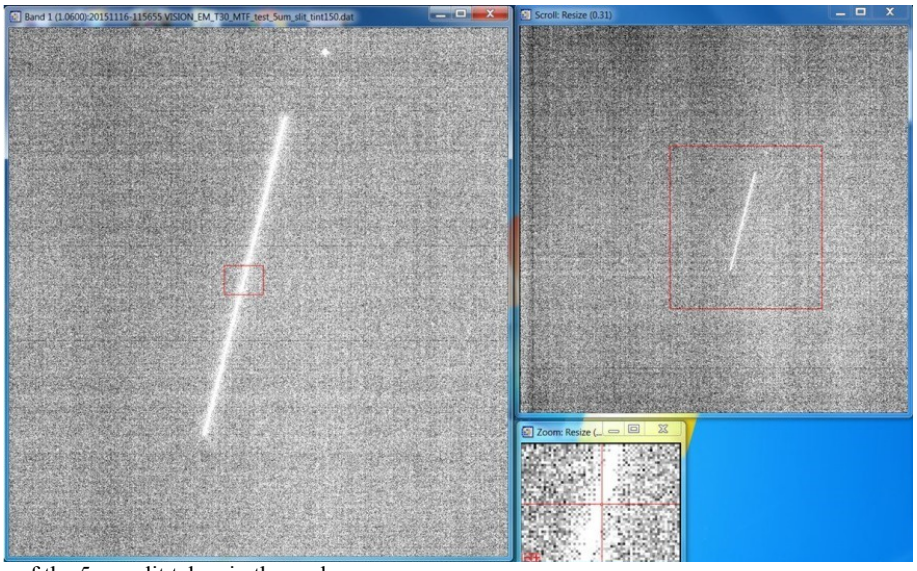

Figure 14. Image of the 5 µm slit taken in thermal vacuum.

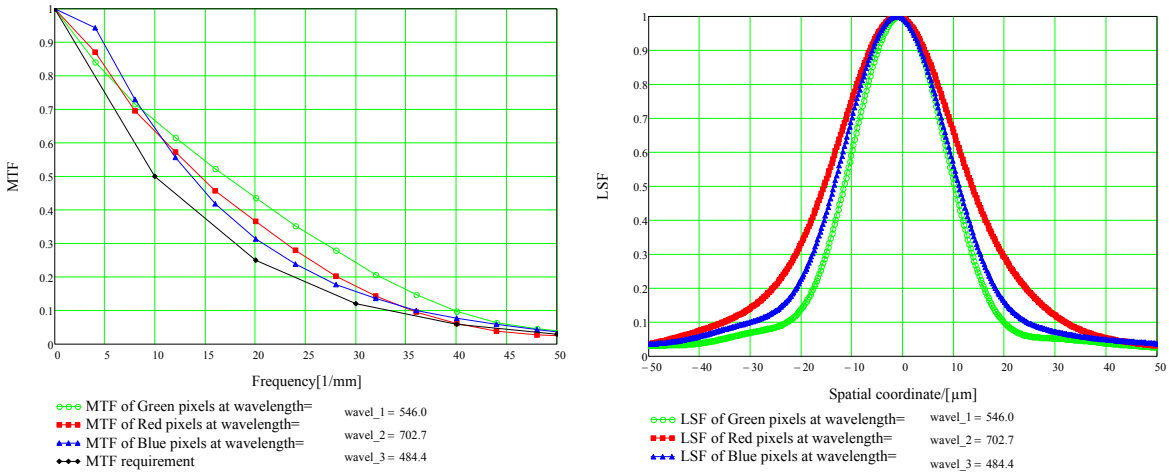

Figure 15. Measured Modulation Transfer Functions (MTF) and Line Spread Functions (LSF) of VISION-EM Green, Red and Blue pixels at wavelengths 546.0, 702.7 and 484.4 nm.

Image sensor performance

The image sensor performance was characterized by a mean-variance measurement at different temperatures. For the measurement, an evenly illuminated target was imaged and then the spatial mean and the reduction variance of two consecutive images were calculated. These values were measured with increasing integration times until the sensor reached saturation state. From this data it is possible to calculate the camera gain (electrons/ADU), the read-out noise (electrons) and the sensor full well (electrons)[6].This measurement was performed in a temperature chamber filled with dry nitrogen atmosphere at temperatures between -42 °C and +50 °C. Image sensor temperatures were ca. 7 degrees higher than the ambient during the measurements. The sensor pre-charge was adjusted during the measurements to achieve adequate image quality at different temperatures. Other sensor parameters were not changed during the test. The main results are shown in Table 2.

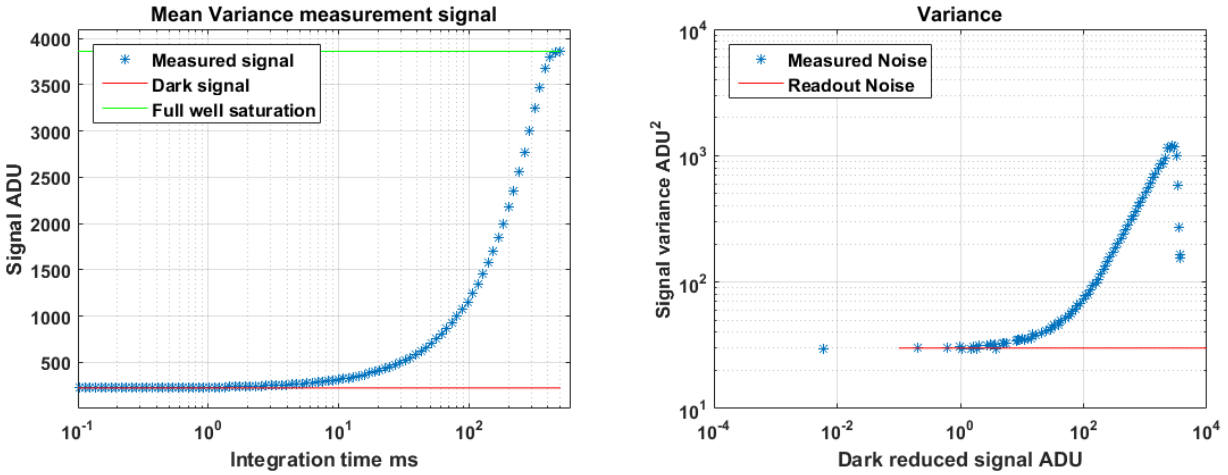

Figure 16. Example data from mean-variance measurement. Figure on the left shows the signal as a function of integration time from dark to saturation and the figure on the right show the signal variance (i.e. noise) in as a function of dark reduced signal.

Table 2. Measured sensor parameters at different temperatures. The camera gain and read noise are not affected by temperature, but the full well and the dark level are affected.

Chamber temp [°C]	Sensor temp [°C]	Average dark level [ADU]	σ	Average full well [e-]	σ	Read noise [e-]	σ	Gain [e-/ADU]	σ	remarks
-42	-35.6	538	N/A	7961	N/A	13	N/A	2.24	N/A	only 2 measurements
-20	-14.0	513	0.8	8420	200	13	0.3	2.35	0.010	
0	5.3	488	1.3	8065	238	13	0.3	2.23	0.013	
25	31.7	447	0.4	8252	13	13	0.1	2.26	0.001	
35	41.3	444	0.8	8171	166	13	0.3	2.24	0.009	
50	57.0	464	0.5	8154	59	13	0.1	2.25	0.003	

The most important result of the measurements is that the camera gain remains stable regardless of temperature. This ensures that the spectral calibration performed at room temperature is also valid at other temperature ranges. The effective full well is affected by the temperature, and the uncertainty in the measurement is pretty high, but no dramatic changes are seen, so the dynamic range remains acceptable over the whole temperature range.

The dark level is also affected; this is mainly due to the sensor characteristics. The CMV4000 is not designed to cover such a wide temperature range with the same settings, and adjustment of sensor pre-charge is required to get good quality images at different temperatures. The downside of this adjustment is that it also changes the offset, which also affects the dark level. The sensor also has a separate offset adjustment, which was not changed during the EM measurements. For the flight model, this parameter will also be tuned for the best performance. As can be seen from the data, the sensor pre-charge adjustment does not affect the readout noise or the camera gain.

Instrument calibration

As the observation principle of VISION is self-calibrating, the absolute radiometric calibration is not required for the instrument. The spectral calibration will provide the information on the absolute radiometric performance at the accuracy of ±35 %.

The spectral calibration requirements are defined for the ISRF (Instrument Spectral Response Function) which is a linear combination of the Red, Green and Blue pixel responses which will be measured. The knowledge of the spectral band central wavelength is dependent on the accuracy of the Bentham monochromator. The band center wavelength accuracy of the Bentham Monochromator TMc300 is ±0.1 nm which is adequate for the VISION calibration.

The spectral calibration is based on illuminating the hyperspectral imager with monochromatic light at a fixed FPI air gap and scanning the wavelength over the relevant range 400 – 850 nm. The image data of the sensor is recorded for all wavelengths. The light source intensity is monitored with a reference photodiode.[4]

During the calibration the measured FWHM values range from 10.9 nm at the lowest FPI order down to 5.5 nm at the highest order. An example of such calibration result is shown in left side of Figure 17. Also the spectral smile, i.e. the variation in wavelength over the image sensor, was measured during the calibration. Spectral smile is mostly 1.6 nm or less. The image of the sun does not extend over the whole image sensor, but approximately 450 pixels x 450 pixels, i.e. around 2 rows x 2 columns of the calibration sub-windows. Therefore the smile over the sun image is much smaller than what is plotted in the right side of Figure 17.

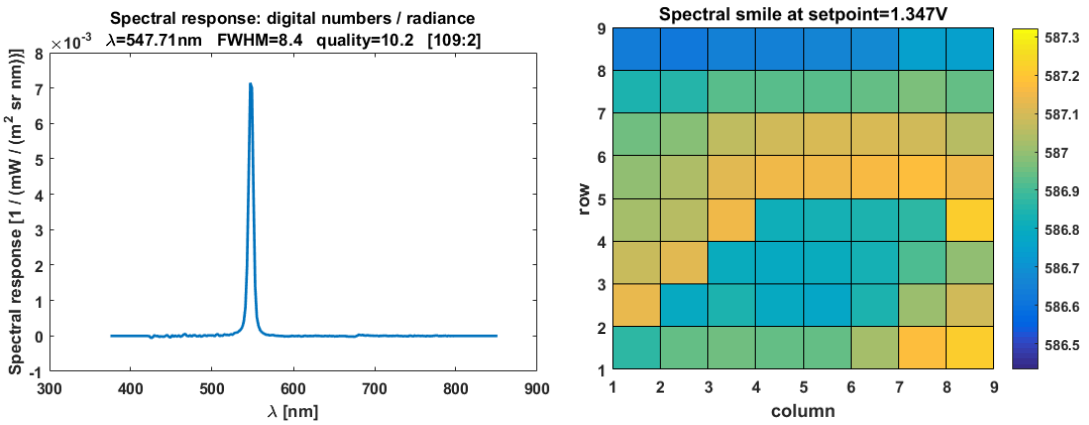

Figure 17. Left: an example of a spectral response function measured during calibration. Right: spectral smile over the image sensor. The sensor is divided into 81 sub-windows (227 pix x 227 pix). The spectral smile over the image sensor at this set point is quite small, less than 1 nm.

Figure 18. Measurement setup for the ground based measurements. VISION-EM (the camera at the rear) and a SWIR spectral camera (the camera at the front) are attached to the tripod. Reference spectrometer for the SWIR camera is also visible (Ocean Optics NIR-Quest).

Ground based measurements

In April 2016 there was an opportunity to perform ground based direct sun measurements with VISION-EM (Figure 18). The conditions were quite clear but windy. In the measurement setup the VISION EM (along with other instruments) was attached to a motorized tripod, which could be programmed to track the sun. The pointing accuracy of the tripod was adequate for the measurements, as the image of the solar disk moved only by few pixels between measurements. The measurements were performed between 14:15 and 14:35 (+0300), so the solar elevation angle was ca. 35 degrees during the measurements. The measured solar spectrum is shown in Figure 19 with comparison to simulated solar spectrum (simulation done by BISA). As the simulation was computed for standard water vapor and aerosol contents, the shape of the spectral continuum is not directly comparable to the measurement, but the strongest features are identifiable in the

measured spectrum. Different aerosol content could explain the lower signal levels at from 500 nm onwards. The strong absorptions in the simulation around 720 nm and 760 nm are caused by water vapor and oxygen. When the absorptions are compared to the measurement, it can be seen that the 720 nm feature is much smaller while the 760 nm feature is similar. This would indicate that the simulation has at least too high H_2O content.

Also the radiometric absolute calibration of VISION-EM was performed at low accuracy because the VISION operation principle is self-calibrating i.e. solar occultation in which the reference spectrum without the atmosphere is always measured and used to retrieve the tangential transmission spectrum of the atmosphere. The absolute radiometric calibration procedure is planned to be improved for the VISION Proto-Flight Model (PFM).

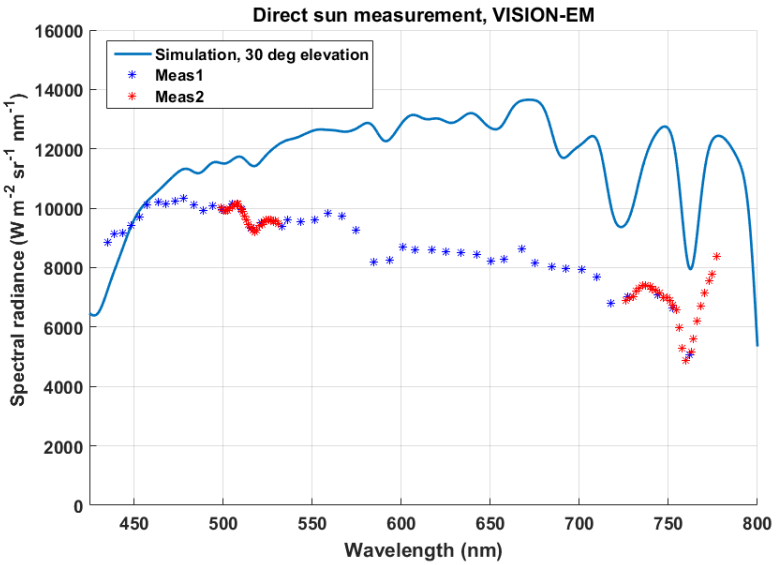

Figure 19. Measured solar spectrum from the roof of the office building in Otaniemi, Finland. The Y-axis is not very well defined, as the absolute calibration of the instrument is not very accurate. The two measurements, taken with two different sets of set points match each other very well.

4. FLIGHT MODEL DEVELOPMENT STATUS

The flight model integration was completed during summer 2016 and the preliminary tests indicate good performance. The design has mostly remained unchanged from the EM, with some improvements based on lessons learned from the EM development. The integrated FM is shown in Figure 20.

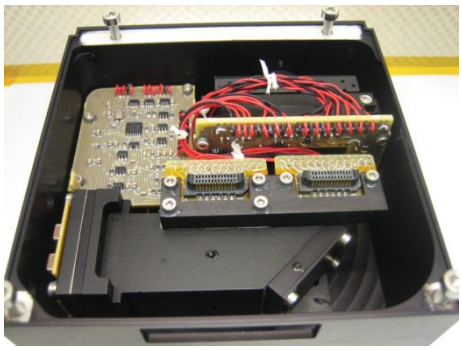

Figure 20. Integrated VISION-PFM without the cover plate and main control PCB.

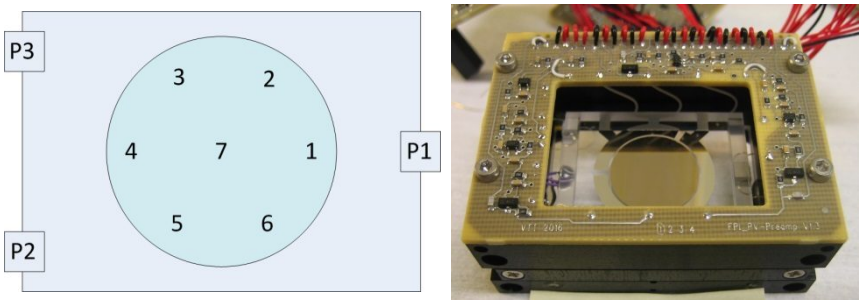

Figure 21. The air gap was measured from seven points, as shown on left. The actual FPI module is shown on the right.

The FPI for the PFM was calibrated and characterized for temperature range between -25 °C and + 50 °C to ensure the high performance operation during the actual mission. The air gap quality was characterized by measuring the air gap width at 7 different locations after the gap was made parallel. The measurement point locations are shown in Figure 21. Any deformations in the air gap generally affect the width of the spectral transmission peak, thus the smaller the deformations are, the better will the spectral performance be.

The peak-to-valley (P-V) is a good measure for the air gap quality. This denotes the difference between the minimum and maximum air gap value within the optical aperture of the FPI. Another related measure is the standard deviation of the air gap within the optical aperture, which tells how much the air gap varies from the mean air gap. Both of these measures are useful for describing the air gap quality, as larger P-V values may still be acceptable if the standard deviation is still small as long as the P-V value is not too large. The measurement data is shown in Figure 22, with a comparison to a previous instrument, the Aalto-1 Spectral Imager (AaSI)[7].

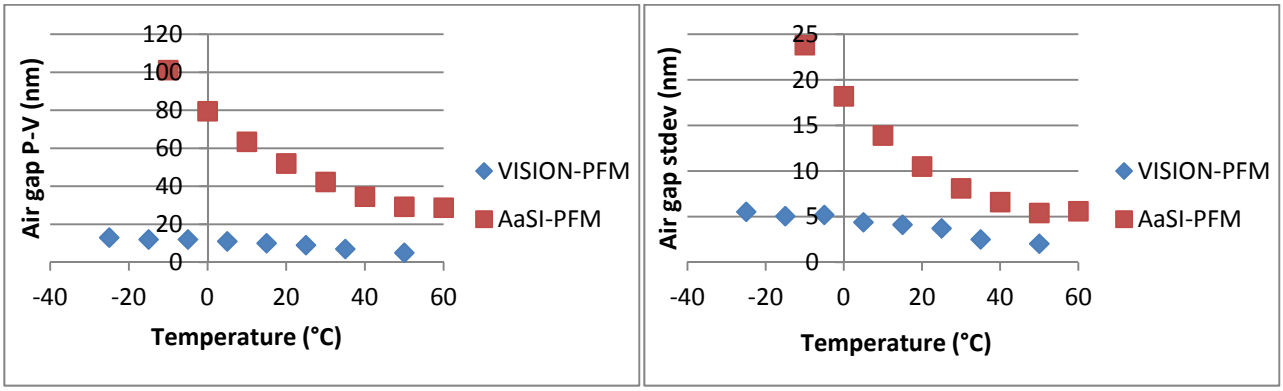

Figure 22. The air gap peak-to-valley (left) and standard deviation (right) of the PFM FPI optical aperture.

The measurement shows that the air gap deforms slightly at colder temperatures, but the P-V is remains less than 15 nm and the standard deviation remains below 6 nm. This means that the spectral performance is not degrading very much with temperature, especially when compared to the earlier instrument. As the FPI was calibrated to parallel air gaps at different temperatures, this data can be used to create a more efficient active temperature compensation for the VISION-PFM to improve the spectral stability and performance.

5. SUMMARY AND CONCLUSIONS

The VISION-EM test campaign has been completed with satisfactory results. The basic design had already been tested with the Aalto-1 Spectral Imager, and the upgrades done on VISION have increased the performance as was hoped. The most important improvement has been the reduced temperature effects on the FPI performance. In earlier designs, the spectral performance of the FPI deteriorated below +10 °C, but in VISION there is no dramatic deterioration even at -35 °C. Also the spectral stability has been improved, especially with the EDGE calibration. The EDGE calibration was also thoroughly tested and according to the results, it seems to be a robust way to correct for the possible short or long term shifts in wavelength.

The ground based measurements of the atmospheric spectrum using direct-sun measurement also look promising. The measured atmospheric resembles the simulated spectrum, and the strongest absorption bands are visible. These measurements will be continued later as the weather permits in order to further characterize the capabilities of the instrument.

The design enables small, robust and lightweight spectral imagers for different nanosatellite missions, as the wavelengths can be freely selected and the wavelength range can be tuned to different application needs. The first spaceflight campaign for the technology will be the Aalto-1 mission, scheduled for launch in late 2016 and the PICASSO mission is scheduled to launch during 2017. These two missions will produce scientific spectral imaging data from CubeSats for the first time.

6. ACKNOWLEDGEMENTS

Work on VISION development has been supported by ESA contract 4000112430/14/NL/MH (GSTP and TRP programs) and the Belgian Science Policy Office. Work at BIRA-IASB on the development of SLP has been sponsored in the context of the Solar-Terrestrial Centre of Excellence by the Belgian Science Policy Office.

REFERENCES

[1] Fussen, D., Pieroux, D., Ranvier, S., De Keyser J., and Cardoen, P., "The PIC.A.S.S.O. mission: A PICo-satellite for Atmospheric and Space Science Observations," 6th European CubeSat Symposium book of abstracts, 19-20 (2014).

[2] Saari, H., Näsilä A., Holmlund C., Mannila R., Näkki I., Ojanen H. J., Fussen D., Pieroux D., Demoulin P., Dekemper E. and Vanhallemont F., " Visible Spectral Imager for Occultation and Nightglow (VISION) for the PICASSO mission", Proc. SPIE 9639 (2015).

[3] Hecht E., [Optics], 4th edition, Addison Wesley, pp.424 (2002).

[4] Saari, H., Aallos, V-V., Akujärvi, A., Antila, T., Holmlund, C., Kantojärvi, U., Mäkynen, J., and Ollila, J., "Novel miniaturized hyperspectral sensor for UAV and space applications", Proc. SPIE 7474 (2009).

[5] Näsilä, A, "Validation of Aalto-1 Spectral Imager Technology to Space Environment", Master's thesis, Aalto University (2013).

[6] Janesick, J. R., [Scientific charge-coupled devices], SPIE, Bellingham & Washington, pp. 101-107 (2001)

[7] Mannila R., Näsilä A., and Saari, H., "Spectral Imager based on Fabry-Perot interferometer for Aalto-1 nanosatellite", Proc. SPIE 8870 (2013).